Chapter 4
Nonlinear Unsharp Masking for Enhancing Suspicious Regions in Mammograms

Yicong Zhou and C. L. Philip Chen
Department of Computer and Information Science, University of Macau, Macau, China

Sos S. Agaian
Department of Electrical and Computer Engineering, University of Texas at San Antonio, San Antonio, TX, USA

Karen Panetta
Department of Electrical and Computer Engineering, Tufts University, Medford, MA, USA

4.1 Introduction

Breast cancer is the leading cause of death in women between the ages of 35 and 55. The National Cancer Institute estimates that one out of eight women in the United States will develop breast cancer at some point during her lifetime.[1] The mortality rate of 30% in the U. S. and 45% in Europe has been demonstrated by repeated, randomized, and controlled trials.[2] Currently, there are no effective ways to prevent breast cancer.[3,4] However, treatments of breast cancer in the early stages are more successful; therefore, early detection is an important and effective method to significantly reduce mortality. There are several imaging techniques for breast examination, including magnetic resonance imaging (MRI), ultrasound imaging, positron emission tomography (PET) imaging, computed tomography (CT) imaging, optical tomography/spectroscopy, and x-ray imaging. Among them, mammography (x-ray image) is the most-common technique that radiologists use to detect and diagnose

breast cancer.[5,6] Two types of mammography are currently used: film mammography and digital mammography. Digital mammography is preferred by physicians[7,8] because it has better image quality, requires a lower x-ray dose,[8] provides interpretations with greater confidence in difficult cases, and offers faster diagnosis for routine cases.[9]

Due to the limitations of the x-ray hardware systems, screened mammograms—even when using digital mammography—may present low resolution or low contrast, making it difficult to detect tumors at an early stage. Important indicators of early breast cancer,[10,11] such as irregularly shaped microcalcifications, are very small calcium deposits that appear as bright, granular spots in mammograms.[12,13] The distinction between the tiny malignant tumors and the benign glandular tissue is not readily discernable; misinterpretation results in unnecessary additional examinations and biopsy.[14] The situation becomes worse when radiologists routinely interpret large numbers of mammograms and can misdiagnose a condition.[15]

To improve the visual quality of mammographic images, more image data can be collected at the data acquisition stage, thus improving the image resolution. However, this significantly increases the overall acquisition time, the amount of radiation that a patient is exposed to, and hardware costs.[16] On the other hand, the image visual quality can be enhanced during the post-image-processing stage in medical imaging systems. It utilizes different image enhancement techniques to enhance the contrast of mammograms. In this way, the visual quality of mammograms is improved without affecting the acquisition process or increasing the hardware costs.

The underlying concept of mammogram enhancement involves applying image enhancement algorithms to improve the contrast of suspicious regions and objects in mammograms, and then use a threshold to separate them from their surroundings.[11] To employ it in the medical imaging system, two problems need to be addressed: (1) How to automatically choose the best enhancement algorithm, and (2) how to automatically select the thresholding.

Several algorithms for mammogram enhancement have been developed recently. They can be classified into two main categories: frequency domain methods and spatial domain methods.

- **Frequency domain methods** are based on different transforms or fuzzy logic theory. These transforms include the discrete Fourier transform (DFT),[17–23] discrete cosine transform (DCT),[24–26] discrete wavelet transform (DWT),[27–44] and other transforms.[23,26,45,46]

  The DWT-based enhancement algorithms for mammograms first decompose mammograms into a multiscale subband representation using the contourlet transform[30] or other wavelet transforms such as the discrete dyadic wavelet transform,[31,33–35] integrated wavelets,[36] or redundant discrete wavelet transform.[37] Next, the transform coefficients in each subband of the multiscale representation are modified using different technologies, including nonlinear filtering,[38] regression-based

extrapolation,[39] adaptive unsharp masking,[40] the wavelet shrinkage function,[41] or direct contrast modification.[42] Finally, the enhanced mammograms can be obtained from the modified coefficients. However, it has been reported that a wavelet representation does not efficiently show the contours and the geometry of edges in images.[30]

Fuzzy set theory has been used to enhance the contrast of mammograms because it is suitable for dealing with the uncertainty associated with the definition of image edges, boundaries, and contrast.[4,47–49] Fuzzy logic has also been successfully integrated with other techniques such as histogram equalization for enhancing medical images[48] and structure tensor for contrast enhancement of micro-calcifications in digital mammograms.[49] However, the frequency domain methods have limitations. They may introduce artifacts called "objectionable blocking effects"[17] or enhance images globally but not enhance all local details/regions in the image very well. Furthermore, it is very difficult to apply them to automatic image enhancement procedures.[18,19]

- **Spatial domain methods** are based on the human visual system (HVS),[50–53] empirical decomposition,[54–57] histogram equalization,[48,52,58–62] logarithmic framework,[63–66] nonlinear filtering,[43,53,67–70] adaptive neighborhood,[9,15,71,72] or unsharp masking.[73–75]

  Because nonlinear filtering is known for its ability to obtain more robust characteristics for suppressing noise and preserving edges and details, it is a desirable technique that can be used to enhance mammographic images and other types of medical images. Examples include utilizing the adaptive density-weighted filter,[67] tree-structured nonlinear filters,[43] and also adaptive anisotropic filtering.[76]

  Several other algorithms have been developed for mammogram enhancement using adaptive neighborhood (or region-based) contrast enhancement (ANCE).[9,15,71,72] ANCE is intended to improve the contrast of specific regions, objects, and details in mammograms based on the local-region background and contrast. The region contrast is calculated and enhanced according to the region's contrast, its background, its neighborhood size, and its seed pixel value.[9]

  Unsharp masking (UM) is another interesting enhancement technique belonging to spatial domain methods. The traditional UM has good performance to enhance the fine details in the original images. However, it also amplifies noise and overshoots the sharp details at the same time.[75,77] To overcome this problem, several modification schemes have been developed by replacing the high-pass filter with the adaptive filter,[77] quadratic filter,[78] and its derived filtering operators, called rational unsharp masking[75] and cubic unsharp masking.[79] Other algorithms using unsharp masking techniques for mammogram enhancement have been developed.[40,73,74] A set of measure metrics for mammogram enhancement is introduced in Singh and Bovis.[80]

This chapter introduces a new nonlinear unsharp masking (NLUM) scheme for mammogram enhancement by combining the nonlinear filtering and unsharp masking techniques. Leveraging the advantages of these two techniques, the new scheme can enhance the contrast of suspicious regions, objects, and details to achieve better visibility of mammographic images for human observers (radiologists). Furthermore, to address the two questions posed earlier concerning the automatic selection of the best enhancement algorithm and of the threshold, a new enhancement measure called the second-derivative-like measure of enhancement (SDME) is introduced. Different parameters in the enhancement algorithm are varied, and the results are measured automatically to choose the best one to present. The NLUM enhancement performance is demonstrated by comparison with other existing enhancement algorithms, quantitative evaluation using the SDME measure, and receiver operating characteristic (ROC) analysis based on a medical doctor's inspection.

Section 4.2 reviews several existing enhancement algorithms that are to be compared with the new NLUM scheme, and the operations of the parameterized logarithmic image processing (PLIP) to be consistent with the human visual system. Section 4.3 introduces the new NLUM scheme. Section 4.4 introduces the new enhancement measure after reviewing several existing ones for quantitatively evaluating the performance of enhancement algorithms. Section 4.5 shows the parameter design and optimization for the NLUM scheme using the SDME measure, compares the NLUM scheme with three existing enhancement algorithms, and evaluates the NLUM using the thresholding technique and ROC analysis. Section 4.6 reaches a conclusion.

4.2 Background

This section briefly discusses traditional unsharp masking and four existing enhancement algorithms including rational unsharp masking (RUM),[75] adaptive neighborhood contrast enhancement (ANCE),[9] contrast-limited adaptive histogram equalization (CLAHE),[58] and direct image contrast enhancement (DICE).[42] Those algorithms will form the basis for comparison to the new NLUM scheme. The arithmetic operations of parameterized logarithmic image processing (PLIP) are also presented here and will be used as an operator in the presented NLUM scheme to better represent the human visual system response.

4.2.1 Traditional unsharp masking

The foundation of the traditional unsharp masking (UM) technique involves subtracting a low-pass filtered signal from its original. The same results can be achieved by adding a scaled high-frequency part of the signal to its original. This is equivalent to adding the scaled gradient magnitude back to the original signal.[78]

The unsharp masking is used to improve the visual quality of images by emphasizing their high-frequency portions that contain fine details as well as

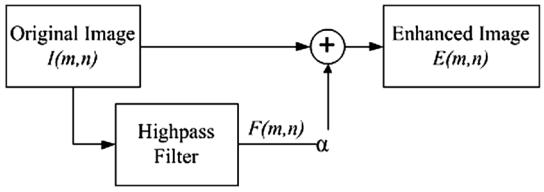

Figure 4.1 The block diagram of the traditional unsharp masking.

noise and sharp details. The scheme for image enhancement is shown in Figure 4.1.

The output enhanced image $E(m,n)$ is defined by

$$E(m,n) = I(m,n) + \alpha F(m,n), \tag{4.1}$$

where the constant α is a scaling factor, and $F(m,n)$ is a high-pass filtered image obtained from the original $I(m,n)$.

The high-pass filter and scaling process in traditional UM amplify those high-frequency portions of original images that contain fine details as well as noise and sharp details. Therefore, due to the fact that traditional UM enhances fine details in images, it also amplifies noise while overenhancing the steep edges.

4.2.2 The RUM algorithm

Rational unsharp masking[75] (RUM) uses a rational function operator to replace the high-pass filter in traditional unsharp masking, shown in Figure 4.2. The rational function is the ratio of two polynomials of the input variables. This scheme is intended to enhance the details in images containing low and medium sharpness without significantly amplifying the noise or affecting the steep edges. The enhanced image is defined by

$$E(m,n) = I(m,n) + \lambda[C_x(m,n)F_x(m,n) + C_y(m,n)F_y(m,n)], \tag{4.2}$$

where λ is the scaling factor, and

$$C_x(m,n) = \frac{[I(m,n+1) - I(m,n-1)]^2}{k[I(m,n+1) - I(m,n-1)]^4 + h}, \tag{4.3}$$

$$C_y(m,n) = \frac{[I(m+1,n) - I(m-1,n)]^2}{k[I(m+1,n) - I(m-1,n)]^4 + h}, \tag{4.4}$$

$$F_x(m,n) = 2I(m,n) - I(m,n-1) - I(m,n+1), \tag{4.5}$$

$$F_y(m,n) = 2I(m,n) - I(m-1,n) - I(m+1,n), \tag{4.6}$$

where k and h are proper positive factors.

4.2.3 The ANCE algorithm

The adaptive neighborhood contrast enhancement (ANCE) method[9] was developed to improve the contrast of objects and features with varying sizes and shapes. In this algorithm, each pixel in an image is considered a seed pixel for a region-growing process. Including those neighboring pixels whose gray values are within a specified gray-level deviation (known as the growth tolerance k) from the seed, a local region—called the foreground—is generated around the seed pixel. Another region—called the background—consists of those neighboring pixels that are outside the range of a specified gray-level deviation. The background, which surrounds the foreground, contains nearly the same number of pixels as the foreground. The region contrast is defined by

$$C = \frac{f-b}{f+b}, \tag{4.7}$$

where f and b are the mean gray-level value of the foreground and background, respectively.

The contrast equation in Eq. (4.7) is similar to Weber's ratio[59] $W = \Delta L/L$, where ΔL is the luminance difference between the central region and the overall image luminance L. The minimum contrast of the region is $C_{\min} = k/2$, and k is the growth tolerance. A Weber's rate of approximately 0.02 for a just-noticeable object under standard light conditions indicates that the growth tolerance should be at most 0.04 if regions or objects are to be distinguishable from their background.

The region's contrast is enhanced by increasing its foreground value when the following conditions are satisfied:

1. The region's contrast is low, i.e., $0.02 \leq C \leq 0.4$; and
2. The pixels in the region's background have a standard deviation normalized by their mean values less than 0.1.

The background in the second condition is defined as a region three pixels thick, molded to the original region in shape. The new foreground value is defined by

$$f' = b\frac{1+C'}{1-C'}, \tag{4.8}$$

where C' is the increased contrast based on an empirical look-up table described by Morrow et al.[9]

Therefore, only regions with low contrast are enhanced, whereas the high-contrast regions, such as steep edges, remain unaffected. In order to save computational costs, the redundant pixels in the foreground regions, which have the same values as the seed pixels, are changed to the same new values.

4.2.4 The CLAHE algorithm

The contrast-limited adaptive histogram equalization[58] (CLAHE) is a well-known technique for adaptive contrast enhancement. The normal and adaptive histogram equalizations enhance images using the integration operation. This operation yields large values in the enhanced image if the histogram of the nearly uniform regions of the original image contain several high peaks. As a result, those enhancement methods may overenhance noise and sharp regions in the original images. To solve this problem, the CLAHE algorithm uses a clip level to limit the local histogram in such a way that the amount of contrast enhancement for each pixel can be limited. This clip level is a maximum value of the local histogram specified by users. An interactive binary search process is used to redistribute those pixels that are beyond the clip level. The CLAHE algorithm has the following steps:

1. Divide the original image into contextual regions,
2. Obtain a local histogram for each pixel,
3. Clip the histogram based on the clip level,
4. Redistribute the histogram using binary search, and
5. Obtain the enhanced pixel value by histogram integration.

4.2.5 The DICE algorithm

The direct image contrast enhancement (DICE) algorithm was introduced to enhance screening mammograms in the wavelet domain.[42] It directly amplifies the vertical, horizontal, and diagonal subband components of the original image at different levels of the wavelet decomposition and then reconstructs them to obtain the enhanced image.

4.2.6 The PLIP operations

The parameterized logarithmic image processing (PLIP) model was introduced to provide a nonlinear framework for image processing.[64] The PLIP model can process images as absorption filters using the gray-tone function of images, which is a more-precise approach from a human visual system perspective, while keeping the image pixel values within the range $[0, \mu)$. Operations use the human visual system characteristics that are listed in Table 4.1, where $f(i,j)$ is the original image; $g(i,j)$, g, g_1, and g_2 are the gray-tone functions to generate negative photos of the original images; $\widetilde{\oplus}, \widetilde{\Theta}, \widetilde{\otimes}$, and $\widetilde{*}$ are PLIP addition, subtraction, scalar multiplication, and image multiplication, respectively; c and β are constants; and μ, γ, k, and λ are parameters that can be selected as the maximum value of images or other values. Note that the PLIP addition and scalar multiplication use the same parameter γ because the scalar multiplication is an extension of addition, adding the image to itself c times.[63]

Table 4.1 The PLIP operations.

PLIP Operation	Definition
Gray-tone function	$g(i,j) = \mu - f(i,j)$
Addition	$g_1 \,\widetilde{\oplus}\, g_2 = g_1 + g_2 - \frac{g_1 g_2}{\gamma}$
Subtraction	$g_1 \widetilde{\Theta} g_2 = k\frac{g_1 - g_2}{k - g_2}$
Scalar multiplication	$c \,\widetilde{\otimes}\, g = \gamma - \gamma\left(1 - \frac{g}{\gamma}\right)^c$
Image multiplication	$g_1 \,\widetilde{*}\, g_2 = \varphi^{-1}\left(\varphi(g_1) \cdot \varphi(g_2)\right)$, where $\varphi(g) = -\lambda \cdot \ln^{\beta}\left(1 - \frac{g}{\lambda}\right)$, and $\varphi^{-1}(g) = \lambda \cdot \left(1 - \exp\left(\frac{-g}{\lambda}\right)^{1/\beta}\right)$

4.3 Nonlinear Unsharp Masking

Integrating the nonlinear filtering operation with the unsharp masking technique, this section introduces a new unsharp masking scheme, called nonlinear unsharp masking (NLUM), for mammogram enhancement. This is a complex unsharp masking scheme. It is good at enhancing suspicious regions in mammographic images.

4.3.1 The new NLUM scheme

The block diagram of the NLUM scheme is shown in Figure 4.2. The original mammogram $I(m,n)$ is filtered by a nonlinear filter. The filtered mammogram $F(m,n)$ is then normalized and combined with the original mammogram using the fusion #1 and #2 to obtain an enhanced mammogram $E(m,n)$.

The nonlinear filtering operation applies a nonlinear operation to the pixels within a 3×3 window. Depending on the different applications, the filtering operation and fusion #1 and #2 can be selected as the arithmetic operations, the PLIP operations, or the nonlinear operations such as the mean square root or logic operations. This property makes the NLUM scheme more general, meeting more-complicated requirements for different objects and applications.

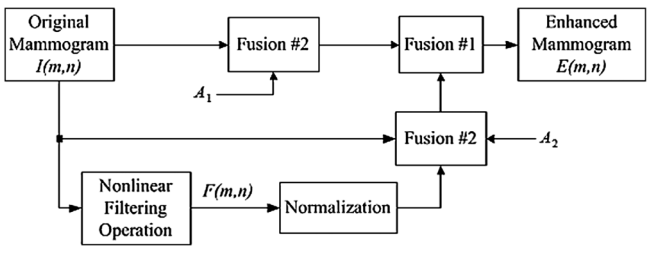

Figure 4.2 Block diagram of the proposed NLUM scheme.

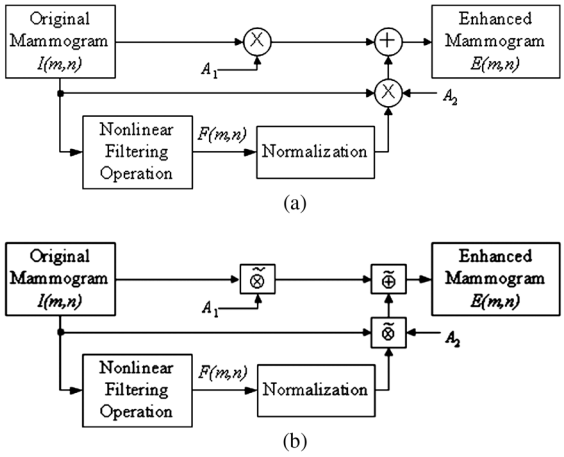

Figure 4.3 Practical examples of the proposed NLUM scheme (a) using the arithmetic operations and (b) using the PLIP operations.

If the NLUM scheme uses the arithmetic operations and fusion #1 and #2 are set to be the arithmetic addition and multiplication, respectively, then the NLUM scheme will resemble the flow shown in Figure 4.3(a). The enhanced mammogram is defined by

$$E(m,n) = A_1 I(m,n) + A_2 \frac{F(m,n)}{|F|_{\max}} I(m,n), \tag{4.9}$$

where A_1 and A_2 are the scaling factors, and $|F|_{\max}$ is the maximum absolute value of the mammogram $F(m,n)$ filtered by a 3×3 nonlinear filter defined by

$$F(m,n) = w_0 I_0 - w_1 I_1 - w_2 I_2, \tag{4.10}$$

where constants $w_0, w_1, w_2 \geq 0$ are weight coefficients, and

$$\begin{aligned} I_0 &= I^{2\alpha_0}(m,n), \\ I_1 &= I^{2\alpha_1}(m-1,n) + I^{2\alpha_1}(m+1,n) + I^{2\alpha_1}(m,n-1) + I^{2\alpha_1}(m,n+1), \\ I_2 &= I^{2\alpha_2}(m-1,n-1) + I^{2\alpha_2}(m+1,n-1) + I^{2\alpha_2}(m+1,n-1) + I^{2\alpha_2}(m+1,n+1), \end{aligned} \tag{4.11}$$

where $\alpha_0, \alpha_1, \alpha_2$ are exponential coefficients, and $I(\bullet)$ is the image pixel intensity value.

On the other hand, if NLUM chooses the PLIP operations and fusion #1 and #2 are selected as the PLIP addition and multiplication, respectively, then the NLUM scheme follows the flow shown in Fig. 4.3(b). The NLUM output will change to

$$E(m,n) = A_1 \widetilde{\otimes} I(m,n) \,\widetilde{\oplus}\, A_2 \widetilde{\otimes} \left(\frac{F(m,n)}{|F|_{\max}} \,\widetilde{*}\, I(m,n) \right), \tag{4.12}$$

where the filtered mammogram $F(m,n)$ is defined as

$$F(m,n) = w_0 \widetilde{\otimes} I_0 \widetilde{\Theta} w_1 \widetilde{\otimes} I_1 \widetilde{\Theta} w_2 \widetilde{\otimes} I_2 \tag{4.13}$$

and

$$\begin{aligned} I_0 &= I^{2\alpha_0}(m,n) \\ I_1 &= I^{2\alpha_1}(m-1,n) \,\widetilde{\oplus}\, I^{2\alpha_1}(m+1,n) \,\widetilde{\oplus}\, I^{2\alpha_1}(m,n-1) \,\widetilde{\oplus}\, I^{2\alpha_1}(m,n+1) \\ I_2 &= I^{2\alpha_2}(m-1,n-1) \,\widetilde{\oplus}\, I^{2\alpha_2}(m+1,n-1) \,\widetilde{\oplus}\, I^{2\alpha_2}(m+1,n-1) \,\widetilde{\oplus}\, I^{2\alpha_2}(m+1,n+1), \end{aligned} \tag{4.14}$$

where $\widetilde{\oplus}, \widetilde{\Theta}, \widetilde{\otimes}, \widetilde{*}$ are PLIP addition, subtraction, scalar multiplication, and image multiplication, respectively, and $A_1, A_2, w_0, w_1, w_2, \alpha_0, \alpha_1, \alpha_2$ are weight coefficients.

A pseudo-code implementation of the NLUM scheme appears below.

```
Input the original image I(m,n)
Set values for parameters A1, A2, w0, w1, w2, α0, α1, α2
    Switch (operation)
    Case: linear operation
        If (Fusion #1 = arithmetic addition) && (Fusion #2 =
        arithmetic multiplication)
            F(m,n) ⇐ apply Eq. (4.2) to input image I(m,n)
            E(m,n) ⇐ Eq. (4.1)
        End
    Case: PLIP operation
        If (Fusion #1 = PLIP addition) && (Fusion #2 = PLIP
        multiplication)
            F(m,n) ⇐ apply Eq. (4.5) to input image I(m,n)
            E(m,n) ⇐ Eq. (4.4)
        End
    End
Output the enhanced image E(m,n)
```

4.3.2 Discussion

NLUM is a complex unsharp masking scheme because there are eight coefficients to be specified for practical applications. However, more coefficients offer NLUM more power and design flexibility to meet more-complex and specific requirements in real-world applications. The nonlinear filtering operation in the NLUM scheme can be designed as a combination of two different types of filters, which offers NLUM more-robust characteristics. For example, the coefficients w_0, w_1, w_2 can be designed as a high-pass filter, and $\alpha_0, \alpha_1, \alpha_2$ can be chosen as a center-weighted mean filter.

The users can manually/experimentally select all of the NLUM coefficients. However, this is a time-consuming method that makes it difficult to reach the best enhancement results due to a lack of criteria for quantitative evaluation. Alternatively, the NLUM coefficients could be

represented by one or two variables based on some reasonable assumptions to simplify the NLUM design and reduce the number of its coefficients in practical applications. An enhancement measure approach could then be used to optimize the coefficients, thus obtaining the best enhancement result. (This method is discussed in Section 4.5.2.)

In summary, the presented new NLUM scheme can be an embodiment of the following scenarios:

1. The fusion operators can be defined as different linear or nonlinear operations.
2. The new nonlinear filtering operator can be designed as a combination of different types of filters.
3. The coefficients allow users to change the NLUM properties to better meet application specific requirements.

These scenarios offer users more design flexibility to adapt the scheme to more specific and complicated requirements in real-world applications. The proposed NLUM can also be applied to other imaging modalities.

4.4 New Enhancement Measure

Developing a good quantitative measure to assess image enhancement is extremely difficult because the improvement in the enhanced images is often subjective and hard to measure. On the other hand, a good quantitative measure is important in order to select the best enhancement results for computer-aided detection (CAD) systems. This section reviews several existing methods of measuring the quality of image enhancement and then introduces a new enhancement measure using the concept of the second derivative.

4.4.1 Discussion

Several measures of image enhancement have been developed by using a contrast measure. The EME (measure of enhancement)[81] and the EMEE (measure of enhancement by entropy) have been developed by Agaian et al.[18] These two measures are based on a Weber-law-based contrast measure. Including the Michelson contrast law,[82] the AME (Michelson–Law measure of enhancement) and AMEE (Michelson–Law measure of enhancement by entropy) were later introduced to improve the measure performance of the EME and EMEE.[19] Because PLIP subtraction has been shown to be consistent with Weber's contrast law and characteristics of the human visual system,[65] the contrast information can be presented and processed more accurately. Including the PLIP operators to further improve these measures, Panetta et al.[51,83] have developed the logAME (logarithmic Michelson contrast measure) and logAMEE (logarithmic AME by entropy). The improved versions of the logAME are the SAME (similarity-based logAME) proposed by Wharton et al.[84] and the Global LogAMEE by Gao et al.[69]

All of these enhancement measures divide an image into $k_1 \times k_2$ blocks and then calculate the average values of the measure results of all blocks in the

Table 4.2 The definition of several enhancement measures.

	Name	Definition
1	Michelson contrast[82]	$C = \frac{I_{\max} - I_{\min}}{I_{\max} + I_{\min}}$
2	EME[18,81]	$EME_{k_1k_2} = \frac{1}{k_1k_2}\sum_{l=1}^{k_1}\sum_{k=1}^{k_2}\left[20\ln\left(\frac{I_{\max,k,l}}{I_{\min,k,l}}\right)\right]$
3	EMEE[18]	$EMEE_{\alpha k_1k_2} = \frac{1}{k_1k_2}\sum_{l=1}^{k_1}\sum_{k=1}^{k_2}\left[\alpha\left(\frac{I_{\max,k,l}}{I_{\min,k,l}}\right)^{\alpha}\ln\left(\frac{I_{\max,k,l}}{I_{\min,k,l}}\right)\right]$
4	AME[19,81]	$AME_{k_1k_2} = -\frac{1}{k_1k_2}\sum_{l=1}^{k_1}\sum_{k=1}^{k_2}\left[20\ln\left(\frac{I_{\max,k,l} - I_{\min,k,l}}{I_{\max,k,l} + I_{\min,k,l}}\right)\right]$
5	AMEE[19]	$AMEE_{\alpha k_1k_2} = -\frac{1}{k_1k_2}\sum_{l=1}^{k_1}\sum_{k=1}^{k_2}\left[\alpha\left(\frac{I_{\max,k,l} - I_{\min,k,l}}{I_{\max,k,l} + I_{\min,k,l}}\right)^{\alpha}\ln\left(\frac{I_{\max,k,l} - I_{\min,k,l}}{I_{\max,k,l} + I_{\min,k,l}}\right)\right]$
6	logAME[51,83]	$\log AME_{k_1k_2} = \frac{1}{k_1k_2}\tilde{\otimes}\sum_{l=1}^{k_1}\sum_{k=1}^{k_2}\left[\frac{1}{20}\tilde{\otimes}\ln\left(\frac{I_{\max,k,l}\tilde{\Theta}I_{\min,k,l}}{I_{\max,k,l}\tilde{\oplus}I_{\min,k,l}}\right)\right]$
7	logAMEE[51,83]	$\log AMEE_{k_1k_2} = \frac{1}{k_1k_2}\tilde{\otimes}\sum_{l=1}^{k_1}\sum_{k=1}^{k_2}\left[\left(\frac{I_{\max,k,l}\tilde{\Theta}I_{\min,k,l}}{I_{\max,k,l}\tilde{\oplus}I_{\min,k,l}}\right)\tilde{*}\ln\left(\frac{I_{\max,k,l}\tilde{\Theta}I_{\min,k,l}}{I_{\max,k,l}\tilde{\oplus}I_{\min,k,l}}\right)\right]$
8	SAME[84]	$SAME_{k_1k_2} = \frac{1}{k_1k_2}\tilde{\otimes}\sum_{l=1}^{k_1}\sum_{k=1}^{k_2}\frac{\lvert I_{\max,k,l}\rvert\tilde{\Theta}\lvert I_{\min,k,l}\rvert}{\lvert I_{\max,k,l}\rvert\tilde{\oplus}\lvert I_{\min,k,l}\rvert}$
9	Global LogAMEE[69]	$\mathrm{Glog}AMEE_{k_1k_2} = \frac{1}{k_1k_2}\tilde{\otimes}\sum_{l=1}^{k_1}\sum_{k=1}^{k_2}\left[\frac{(I_{\max,k,l}\tilde{\Theta}I_{\min,k,l})(I_{\max}\tilde{\oplus}I_{\min})}{(I_{\max,k,l}\tilde{\oplus}I_{\min,k,l})(I_{\max}\tilde{\Theta}I_{\min})}\tilde{*}\ln\left(\frac{(I_{\max,k,l}\tilde{\Theta}I_{\min,k,l})(I_{\max}\tilde{\oplus}I_{\min})}{(I_{\max,k,l}\tilde{\oplus}I_{\min,k,l})(I_{\max}\tilde{\Theta}I_{\min})}\right)\right]$
10	Region contrast[42]	$C_w(I) = \frac{1}{m}\sum_{w}\lvert c(x,y)\rvert\log(1+\lvert c(x,y)\rvert)$, where $c(x,y) = 4I(x,y) - I(x-1,y) - I(x,y-1) - I(x+1,y) - I(x,y+1)$

entire image. The definitions of these measures are listed in Table 4.2, where the image I is divided into $k_1 \times k_2$ blocks, and α is constant. $I_{\max}$ and $I_{\min}$ are the maximum and minimum of the intensity values in these blocks, respectively. However, these enhancement measures only calculate the maximum and minimum values of the small regions or blocks in images. As a result, they are sensitive to noise and to steep edges in images.

Other enhancement measures include region contrast of a region in an image[42] $I(x, y)$ and contrast in the DCT domain.[85] A new enhancement measure is introduced here using the concept of the second derivative because it measures the change ratio of the variation speed of pixel values.

4.4.2 New enhancement measure: SDME

Integrating the idea of the second-derivative-like visibility operator[44] with the strengths of the earlier reviewed measures, a new enhancement measure called the second-derivative-like measure of enhancement (SDME) is introduced here. It is defined by

$$SDME = -\frac{1}{k_1 k_2} \sum_{l=1}^{k_1} \sum_{k=1}^{k_2} 20 \ln \left| \frac{I_{\max,k,l} - 2I_{center,k,l} + I_{\min,k,l}}{I_{\max,k,l} + 2I_{center,k,l} + I_{\min,k,l}} \right|, \tag{4.15}$$

where an image is divided into $k_1 \times k_2$ blocks, $I_{\max,k,l}$, $I_{\min,k,l}$ are the maximum and minimum values of the pixels in each block separately, and $I_{center,k,l}$ is the intensity of the center pixel in each block. Thus, the size of the blocks should be an odd number of pixels, such as 3×3 or 5×5.

Because $I_{center,k,l} \neq \pm\frac{1}{2}(I_{\max,k,l} + I_{\min,k,l})$ according to the SDME definition, the blocks with $I_{center,k,l} = \pm\frac{1}{2}(I_{\max,k,l} + I_{\min,k,l})$ will be discarded when calculating the SDME of an image. Therefore, when $I_{center,k,l}$ approaches $\pm\frac{1}{2}(I_{\max,k,l} + I_{\min,k,l})$, the SDME value will approach infinity; when $I_{center,k,l} = 0$ for all blocks, the minimal SDME value is zero.

4.5 Simulation Results and Evaluations

This section provides experimental results to discuss the SDME measure performance, the NLUM parameter optimization, and the NLUM enhancement analysis, comparison, and evaluation.

4.5.1 Comparison of enhancement measures

The SDME is compared with six existing measure methods. The measure performance of each method is determined by the consistency of the measure results and subjective evaluation of visual quality of mammograms.

The subjective evaluation method uses the mean opinion score (MOS) recommended by the International Telecommunication Union Telecommunication Standardization Sector (ITU-T).[86] The MOS intends to determine which results are the most visually pleasing for a human observer. In this

subjective test, seven human observers visually evaluated all original and enhanced mammograms. Each mammogram was given a MOS score of 1–5, where a score of five indicates the best visual quality.

A set of 19 test mammograms was randomly selected from the Internet and the mini-MIAS database of mammograms.[87] They were enhanced using four algorithms: NLUM, RUM, ANCE, and CLAHE. Therefore, including the original and enhanced mammograms, there were 95 test images in total ($19 \times 5 = 95$) for this comparison. They were evaluated according to the subjective method and enhancement measures.

Table 4.3 shows the average subjective evaluation scores of each observer for the test mammograms. The bottom row lists the average evaluation scores of all human observers on enhanced images categorized by enhancement algorithms. Based on the scores, NLUM gives the best overall visual quality with a score of 4.6857, whereas CLAHE obtains the worst quality with a score of 1.9048.

The SDME and six existing measures are then used to measure the quality of all 95 test images. Each individual enhancement measure has its own data range; a good measure method should yield higher measure results for images with higher visual quality, and vice versa.

As shown in Table 4.4, different measures have diverse evaluation results for these enhancement algorithms. For example, the EME evaluates CLAHE-enhanced images as the best, whereas the AME gives the highest value to the

Table 4.3 Subjective evaluation for the enhanced results by different algorithms. The rating scale: 1 = bad, 2 = poor, 3 = fair, 4 = good, 5 = excellent.

Observer	Original	NLUM	RUM	ANCE	CLAHE
#1	3.5556	4.6111	3.3333	2.6111	1.4444
#2	3.6667	4.9444	3.0000	2.5556	1.7222
#3	3.4444	4.2222	3.1111	2.3889	1.6667
#4	3.7778	4.6889	3.0000	2.3333	2.0000
#5	3.3333	4.8889	3.2222	2.6667	2.6111
#6	3.8889	4.7778	3.2778	2.0000	2.1111
#7	4.1111	4.6667	3.4444	2.4444	1.7778
Average	**3.6825**	**4.6857**	**3.1984**	**2.4286**	**1.9048**

Table 4.4 Comparison of measure results based on different algorithms. For each individual enhancement measure, a higher score indicates better enhancement performance.

Enhancement Measure	Original	NLUM	RUM	ANCE	CLAHE
EME	0.9129	1.0833	1.0024	1.0023	2.5425
EMEE	0.0560	0.0688	0.0715	0.0614	0.1961
AME	26.4940	25.1455	26.3165	25.6358	17.4429
AMEE	0.0611	0.0679	0.0619	0.0653	0.1105
logAME	0.0526	0.0485	0.0522	0.0506	0.0316
logAMEE	0.0894	0.0993	0.0894	0.0942	0.1366
SDME	43.6388	47.2091	43.3729	42.2219	35.5386

original images. Comparing the MOS evaluation results in Table 4.4, the SDME is the only measure whose results are consistent with the MOS evaluation results. The rest of this chapter uses the SDME to assess the enhancement performance of different algorithms.

4.5.2 Parameter optimization

To demonstrate how to design and automatically optimize the NLUM parameters using the proposed SDME, one mammogram obtained from the Internet is used as an example; HVS-based image decomposition is then applied for the visualization and analysis of the enhanced results. The SDME is also used to measure and evaluate the performance of the NLUM for mammogram enhancement.

To assess the enhancement performance of the presented NLUM scheme, the users have the flexibility to use any existing measure approach to establish a qualitative metric of mammogram enhancement. The enhancement measure can also be used to optimize all of the NLUM coefficients to achieve the best enhanced results. Here, the SDME is selected to measure and evaluate the performance of NLUM for mammogram enhancement.

There are eight coefficients in NLUM: To reduce the number of parameters, the user can make assumptions according to the practical design requirements, for example, (1) $A_2 = 1/A_1$, $w_0 = 2$, $\alpha_0 = 8h$, $\alpha_1 = \alpha_2 = h$, and $w_1 = w_2 = -0.125$; or (2) $A_2 = 20A_1$, $w_0 = 8h$, $\alpha_0 = 12h$, $\alpha_1 = h$, $\alpha_2 = 2h$, and $w_1 = w_2 = -h$. These assumptions design the nonlinear filter as a combination of a high-pass filter (w_0, w_1, w_2) and a low-pass filter $(\alpha_0, \alpha_1, \alpha_2)$. More weight is given to the filtered image in order to enhance the fine details in images. With these assumptions, all of the NLUM coefficients are correlated with the parameters A_1 and h. Assumption (1) is selected here to demonstrate how to automatically design NLUM.

By automatically changing the parameters A_1 and h, several enhanced mammograms are generated and then measured by the SDME; the measure results are then plotted as a graph. The parameters giving the best enhanced result can be located at the points where the SDME curve reaches the local extrema.

Different fusion operations can be used in the NLUM scheme; compare the arithmetic operation with the PLIP version. Taking Figure 4.4(a) as a test image, the SDME measure results of the enhanced mammograms by NLUM with arithmetic and PLIP operations are plotted in Figure 4.5. The measure results allow one to find the location of parameters A_1 and h that yield the best enhanced result for each operation.

Using the parameters obtained from the measure in Figures 4.5(a) and (b), the original mammogram is enhanced by NLUM with arithmetic addition and PLIP addition, respectively. The enhanced mammograms and their cropped suspicious regions are shown in Figure 4.4. The visual quality and local contrast of the enhanced mammograms are much better than those of the original. Fine details such as microcalcifications and masses in the original

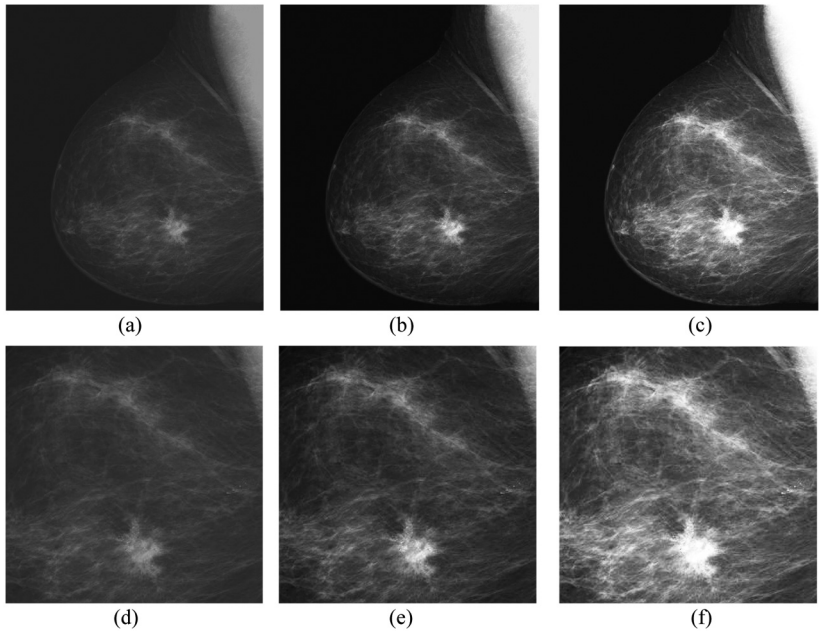

Figure 4.4 Mammogram enhancement: (a) the original mammogram, (b) the NLUM-enhanced mammogram with arithmetic operation, (c) the NLUM-enhanced mammogram with PLIP operation, (d) the cropped region of (a), (e) the cropped region of (b), and (f) the cropped region of (c).

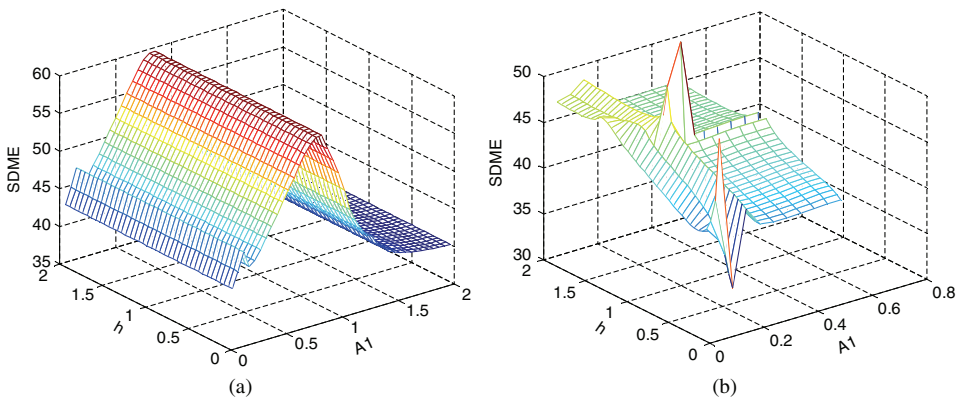

Figure 4.5 The SDME measure plots of mammogram enhancement based on different values of A_1 and h: (a) a SDME measure graph by arithmetic operation and (b) a SDME measure graph by PLIP operation.

mammogram are significantly improved, and the suspicious regions are more recognizable in the enhanced mammograms.

Compared with the enhanced results obtained by using two types of fusion operations in Figure 4.4, the arithmetic operation shows better performance

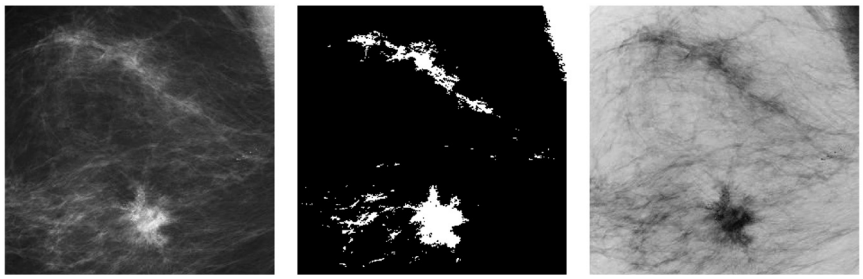

Figure 4.6 Enhancement analysis: (a) the enhanced region cropped from the mammogram in Figure 4.4(b), (b) the threshold image of (a), and (c) the negative photo of (a).

because the NLUM based on PLIP operation slightly overenhances the mass region, as shown in Figure 4.4(c). Therefore, the arithmetic operation is chosen for NLUM to enhance mammograms in the rest of this chapter.

4.5.3 Enhancement analysis

There are many different methods used to analyze the enhanced images. Figure 4.6 provides two examples: the negative view and thresholding of the specific region of interest (ROI). The shape of the suspicious regions is very clear and easily discernable. This demonstrates that NLUM performs well in improving the contrast of suspicious regions, objects, and details in mammograms.

4.5.4 HVS-based analysis and visualization

While the user can view the entire image's enhanced results, the process would be improved if only the suspicious regions could be emphasized during analysis. Instead of using the segmentation algorithms, HVS-based decomposition can be used as an alternative method to provide visualization of results that isolate ROIs, mainly suspicious regions.

By using the background intensity and the rate of information change, HVS-based decomposition separates images into four subimages based on four defined regions: (1) region 1: the saturation region for overilluminated areas; (2) region 2: the Weber region for properly illuminated areas; (3) region 3: the Devries–Rose region for underilluminated areas; (4) region 4: the fourth region for all pixels containing the least informative pixels.[88,89] This section extends its application to enhancement analysis and visualization.

Figures 4.7 and 4.8 show the HVS-based decomposition results of the enhanced mammogram and its negative (tonal inversion), respectively. In general, the mass regions can be segmented by HVS-based decomposition in one subimage without involving any segmentation algorithms. The results are shown in Figures 4.7(b) and 4.8(d). Therefore, HVS-based decomposition can be used for segmentation and classification of pathological cases in a CAD system.

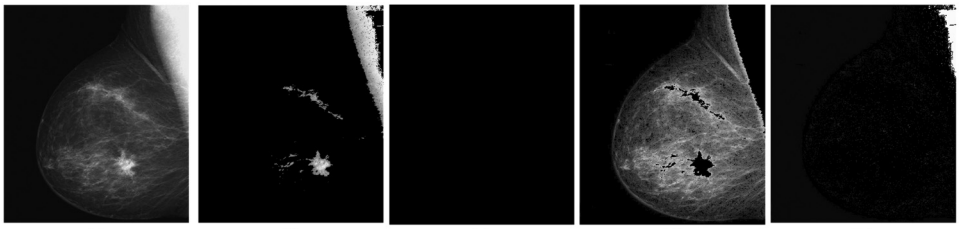

Figure 4.7 HVS-based decomposition of the enhanced mammogram: (a) the enhanced mammogram, (b) the first subimage, (c) the second subimage, (d) the third subimage, and (e) the fourth subimage.

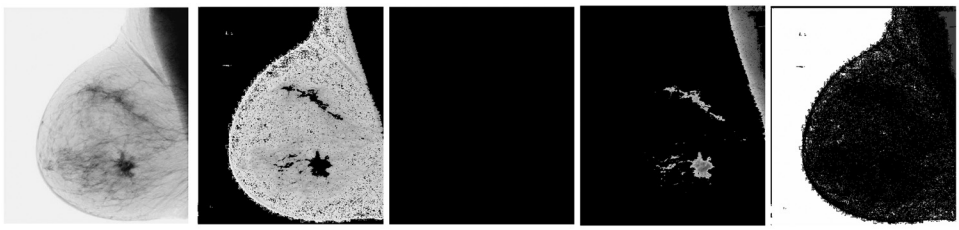

Figure 4.8 HVS-based decomposition of the inversed mammogram: (a) the negative of the image of the enhanced mammogram; (b) the first subimage; (c) the second subimage; (d) the third subimage; and (e) the fourth subimage.

4.5.5 Comparison of enhancement performance

After demonstrating how to automatically optimize the parameters in NLUM, this section applies it to more mammograms and compares it with other well-known enhancement algorithms.

The mammograms for this comparison were obtained from the mini-MIAS database of mammograms.[87] The database consists of 322 mammograms, and the cases of patient records range from fairly dense to extraordinarily dense breast parenchyma. Some cases are completely fatty. Most masses are ill-defined, indistinct, or speculated.

All test mammograms are cropped into smaller-size images for analysis such that the resulting cropped mammographic images contain most of the microcalcifications, masses, and suspicious regions that may be interesting to radiologists. These mammograms have a limited black background, which contains nonobject regions and background project noise.

Six mammograms were used as examples, and the enhanced results are shown in Figures 4.9 and 4.10. They clearly show how the enhancement algorithms change fine details and suspicious regions in images. Their SDME results are shown in Table 4.5.

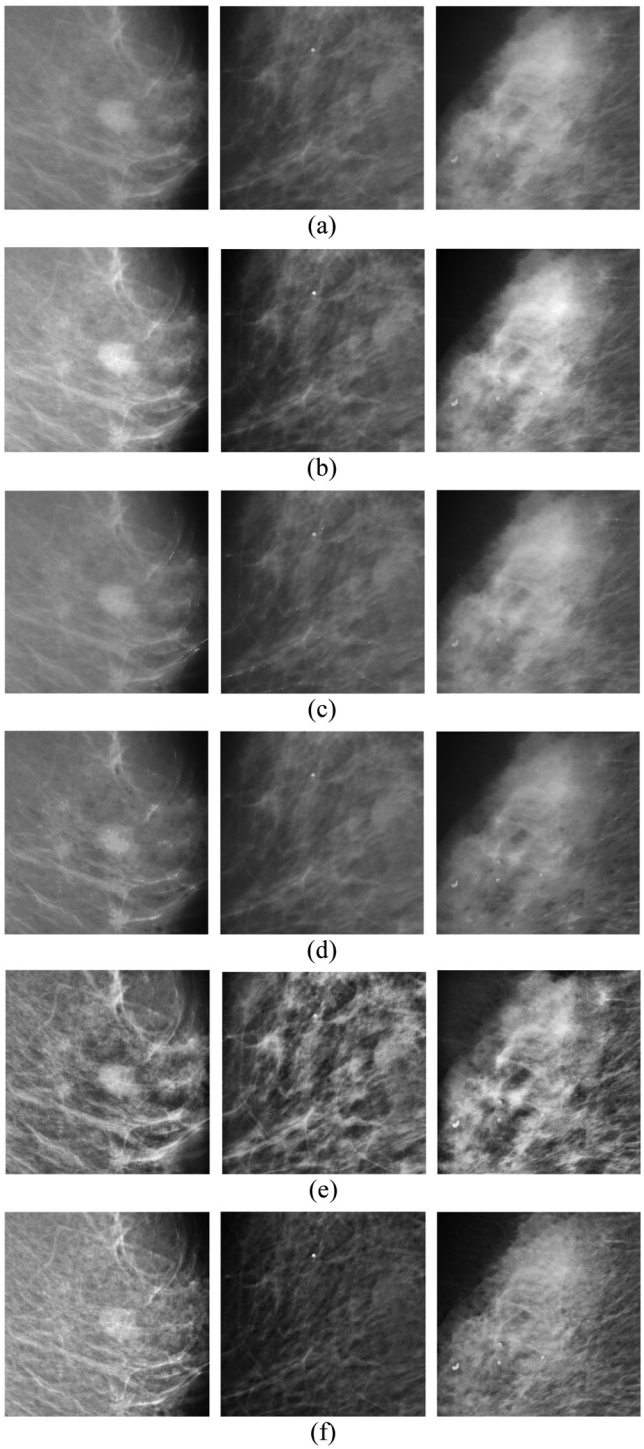

Figure 4.9 Comparison of mammogram enhancement using different algorithms: (a) Original mammograms (Mam_1 to Mam_3), (b) NLUM-enhanced results, (c) RUM-enhanced results, (d) ANCE-enhanced results, (e) CLAHE-enhanced results, and (f) DICE-enhanced results.

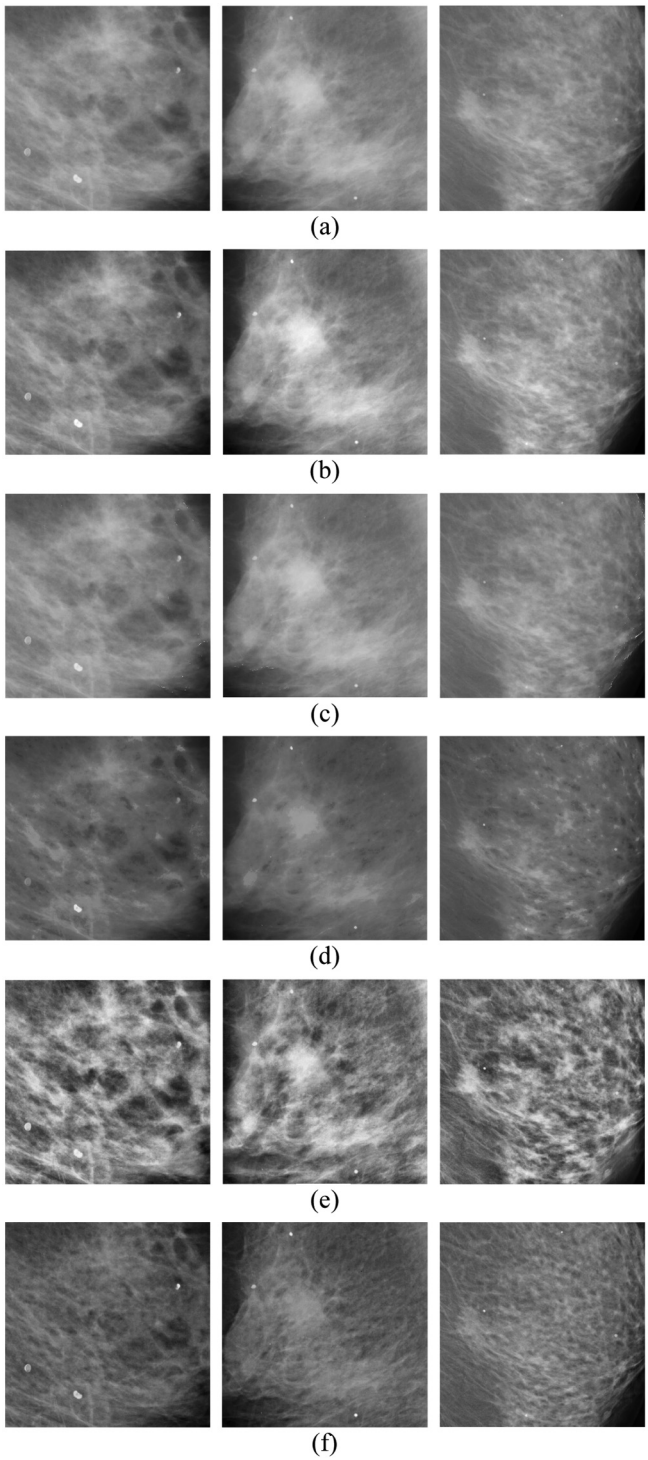

Figure 4.10 Comparison of mammogram enhancement using different algorithms: (a) Original mammograms (Mam_4 to Mam_6), (b) NLUM-enhanced results, (c) RUM-enhanced results, (d) ANCE-enhanced results, (e) CLAHE-enhanced results, and (f) DICE-enhanced results.

Table 4.5 SDME results of mammograms enhanced by different algorithms. A higher score indicates better enhancement performance.

	Original	NLUM	RUM	ANCE	CLAHE	DICE
Mam_1	44.7378	47.4100	44.5905	41.9886	36.1296	39.748
Mam_2	42.4422	44.7627	42.1725	42.4422	34.2108	37.12654
Mam_3	44.1716	46.9127	44.1132	42.0401	35.8518	39.03196
Mam_4	45.3980	47.6609	45.2934	42.0689	36.2382	39.94165
Mam_5	46.7206	49.7931	46.6719	44.6588	37.5773	41.72588
Mam_6	45.0838	47.6866	44.9040	42.1152	35.9426	39.9139

- RUM slightly improves the visual quality of images, but it generates spot artifacts, as shown in Figures 4.8(c) and 4.9(c).
- ANCE has very limited visual improvement and produces many textile artifacts in the mammograms.
- CLAHE overenhances the background of all mammograms, making microcalcifications and/or masses more unrecognizable than the original ones.
- As evident from Figures 4.9(f) and 4.10(f), DICE improves the contrast of the microcalcifications, but it fails to enhance mass regions. It also generates background noise and textile artifacts.

The measure results in Table 4.5 support these observations. The presented NLUM outperforms the others because it improves the contrast of mammograms and visual quality of suspicious regions such as masses and/or microcalcifications, which is useful for detecting and diagnosing diseases or breast cancer at an early stage. The enhanced mammograms have no detail information loss. The measure results in Table 4.5 verify the excellent enhancement performance of NLUM.

4.5.6 ROC evaluation

The receiver operating characteristic curve was originally developed for signal-detection theory. It is a well-known evaluation methodology used for medical decision making and medical diagnostic imaging systems.[90,91] The ROC curve is a graphical plot of the true positive rate (a fraction of true positives over the positives) versus the false positive rate (a fraction of false positives over the negatives). To determine whether a person has a specific disease in the clinical diagnosis, a true positive case occurs when the person tests positive and actually has the disease. A false positive case, on the other hand, occurs when the person tests positive but does not actually have the disease.[92] The MATLAB® implementation of the ROC analysis is addressed in references.[93,94]

This section uses the ROC curve to evaluate the NLUM enhancement performance. 60 mammograms were selected from the mini-MIAS database. They consist of 30 normal mammograms (which do not contain suspect

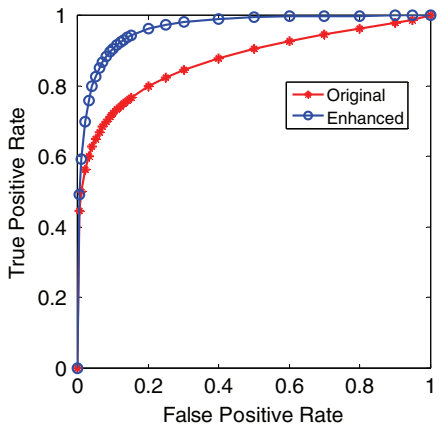

Figure 4.11 The ROC curves of the original and enhanced test mammograms.

regions such as calcifications and masses) and 30 suspicious mammograms. All mammograms were cropped into smaller-size images such that the resulting images have minimal background or contain most of abnormal regions such as microcalcifications and masses.

All mammograms were enhanced by NLUM and then divided in two groups: original and enhanced mammograms. They were inspected by a medical doctor who has a great deal of clinical experience with viewing mammograms. The doctor marked each mammogram with the case type ('0' for the truly negative case indicating a completely normal mammogram and '1' for the truly positive case referring to an abnormal mammogram.) and the confidence rate for each case type. The confidence rate is from 1–5, where '1' indicates a definitely negative case, and '5' means definitely positive.[94]

Using an online code of the ROC analysis developed by Eng,[94] the doctor's inspection results were individually plotted into ROC curves for the original and enhanced mammograms. The results are shown in Figure 4.11.

The area under the ROC curve (AUC) is used to quantitatively evaluate the classification performance of the diagnosis system.[90,91] The AUC value is always between 0 and 1. A higher AUC value indicates better classification performance. The AUC for the enhanced mammogram is 0.957, whereas the AUC for the originals is 0.874. This demonstrates that the NLUM enhancement improves the doctor's diagnosis. It could potentially improve cancer breast diagnosis and detection in the CAD systems.

4.6 Conclusion

This chapter introduced a new nonlinear unsharp masking scheme for mammogram enhancement. NLUM has been shown to provide more design

flexibility that makes it possible to meet more specific and complex requirements in real world applications. The simulation results have demonstrated that the NLUM parameters can be optimized by the enhancement measure to obtain the better enhanced result for clinical applications. Enhancement comparison has proven that the NLUM shows better performance for improving the local contrast of suspicious regions and fine details in mammograms. NLUM has potential applications of improving the automatic disease detection and diagnosis in CAD systems.

To quantitatively evaluate NLUM performance for mammogram enhancement, we have introduced a new enhancement measure called the second-derivative-like measure of enhancement. Compared with other existing measure methods, the SDME shows better performance for enhancement measurement and assessment. HVS-based decomposition has been verified to be a useful tool to analyze and display suspicious regions in mammograms.

References

1. L.-M. Wun, R. M. Merrill, and E. J. Feuer, "Estimating lifetime and age-conditional probabilities of developing cancer," *Lifetime Data Analysis* **4**, 169–186 (1998).
2. D. B. Kopans, "The 2009 U. S. Preventive Services Task Force guidelines ignore important scientific evidence and should be revised or withdrawn," *Radiology* **256**, 15–20 (2010).
3. D. E. Stewart et al., "Attributions of cause and recurrence in long-term breast cancer survivors," *Psycho-Oncology* **10**, 179–183 (2001).
4. H. D. Cheng and H. Xu, "A novel fuzzy logic approach to mammogram contrast enhancement," *Information Sciences* **148**, 167–184 (2002).
5. R. Mousa, Q. Munib, and A. Moussa, "Breast cancer diagnosis system based on wavelet analysis and fuzzy-neural," *Expert Systems with Applications* **28**, 713–723 (2005).
6. X. Gao, Y. Wang, X. Li, and D. Tao, "On Combining Morphological Component Analysis and Concentric Morphology Model for Mammographic Mass Detection," *IEEE Trans. Information Techn. Biomed.* **14**, 266–273 (2010).
7. R. A. Smith, V. Cokkinides, and H. J. Eyre, "American Cancer Society guidelines for the early detection of cancer 2006," *CA Cancer J. Clin.* **56**, 11–25 (2006).
8. S. A. Feig and M. J. Yaffe, "Digital mammography," *Radiographics* **18**, 893–901 (1998).
9. W. M. Morrow, R. B. Paranjape, R. M. Rangayyan, and J. E. L. Desautels, "Region-based contrast enhancement of mammograms," *IEEE Trans. Med. Imaging* **11**, 392–406 (1992).

10. L. Wei, Y. Yang, M. N. Wernick, and R. M. Nishikawa, "Learning of perceptual similarity from expert readers for mammogram retrieval," *IEEE J. Selected Topics Signal Process.* **3**, 53–61 (2009).
11. J. Tang, R. M. Rangayyan, J. Xu, I. E. Naqa, and Y. Yang, "Computer-aided detection and diagnosis of breast cancer with mammography: recent advances," *IEEE Trans. Information Tech. Biomed.* **13**, 236–251 (2009).
12. H. Li, K. J. R. Liu, and S. C. B. Lo, "Fractal modeling and segmentation for the enhancement of microcalcifications in digital mammograms," *IEEE Trans. Med. Imaging* **16**, 785–798 (1997).
13. S. Halkiotis, T. Botsis, and M. Rangoussi, "Automatic detection of clustered microcalcifications in digital mammograms using mathematical morphology and neural networks," *Signal Process.* **87**, 1559–1568 (2007).
14. S. Timp, C. Varela, and N. Karssemeijer, "Computer-aided diagnosis with temporal analysis to improve radiologists' interpretation of mammographic mass lesions," *IEEE Trans. Information Tech. Biomed.* **14**, 803–808 (2010).
15. R. M. Rangayyan et al., "Improvement of sensitivity of breast cancer diagnosis with adaptive neighborhood contrast enhancement of mammograms," *IEEE Trans. Information Tech. Biomed.* **1**, 161–170 (1997).
16. I. Larrabide, A. A. Novotny, R. A. Feij´oo, and E. Taroco, "A medical image enhancement algorithm based on topological derivative and anisotropic diffusion," *Proc. XXVI Iberian Latin-American Congress on Computational Methods in Engineering*, Guarapari, Esp´irito Santo, Brazil (2005).
17. S. Aghagolzadeh and O. K. Ersoy, "Transform image enhancement," *Opt. Eng.* **31**(3), 614–626 (1992) [doi: 10.1117/12.56095].
18. S. S. Agaian, K. Panetta, and A. M. Grigoryan, "Transform-based image enhancement algorithms with performance measure," *IEEE Trans. Image Process.* **10**, 367–382 (2001).
19. S. S. Agaian, B. Silver, and K. A. Panetta, "Transform coefficient histogram-based image enhancement algorithms using contrast entropy," *IEEE Trans. Image Process.* **16**, 741–758 (2007).
20. A. M. Grigoryan and S. S. Agaian, *Multidimensional Discrete Unitary Transformations: Representation, Partitioning, and Algorithms*, Marcel Dekker, New York (2003).
21. S. S. Agaian, V. Sridharan, and M. Blanton, "Switching system for image enhancement and analysis of fused thermal and RGBD data," *Proc. SPIE* **8406**, 84060Z (2012) [doi: 10.1117/12.924755].
22. J. Xia, K. Panetta, and S. Agaian, "Color image enhancement algorithm based on logarithmic transform coefficient histogram," *Proc. SPIE* **7870**, 78700Y (2011) [doi: 10.1117/12.872418].

23. A. Grigoryan and S. Agaian, "Image Enhancement," in *Advances in Imaging and Electron Physics* **130**, Academic Press, New York, pp. 165–243 (2004).
24. K. Panetta, J. Xia, and S. Agaian, "Color image enhancement based on the discrete cosine transform coefficient histogram," *J. Electron. Imaging* **21**(2), 021117 (2012) [doi: 10.1117/1.JEI.21.2.021117].
25. X. Junjun, K. Panetta, and S. Agaian, "Color image enhancement algorithms based on the DCT domain," *Proc. IEEE SMC2011*, 1496–1501 (2011).
26. S. Krishnan, S. Agaian, D. Mecke, S. A. Montelongo, and X. Wang, "Method and architecture for quantification of bone structure using microscopic image slices," *Proc. SPIE* **8655**, 865517 (2013) [doi: 10.1117/12.2005120].
27. S. Nercessian, S. S. Agaian, and K. A. Panetta, "Multi-scale image enhancement using a second derivative-like measure of contrast," *Proc. SPIE* **8295**, 82950Q (2012) [doi: 10.1117/12.906494].
28. S. C. Nercessian, K. A. Panetta, and S. S. Agaian, "Multiscale image fusion using an adaptive similarity-based sensor weighting scheme and human visual system-inspired contrast measure," *J. Electron. Imaging* **21**(2), 021112 (2012) [doi: 10.1117/1.JEI.21.2.021112].
29. J. Xia, K. Panetta, and S. Agaian, "Wavelet transform coefficient histogram-based image enhancement algorithms," *Proc. SPIE* **7708**, 770812 (2010) [doi: 10.1117/12.855563]
30. Z. Lu, T. Jiang, G. Hu, and X. Wang, "Contourlet based mammographic image enhancement," *Proc. SPIE* **6534**, 65340M (2007) [doi: 10.1117/12.741340].
31. A. Laine, J. Fan, and W. Yang, "Wavelets for contrast enhancement of digital mammography," *IEEE Eng. Med. Biol. Mag*. **14**, 536–550 (1995).
32. A. Laine, W. Huda, B. G. Steinbach, and J. C. Honeyman, "Mammographic image processing using wavelet processing techniques," *Eur. Radiol*. **5**, 518–523 (1995).
33. A. F. Laine, S. Schuler, F. Jian, and W. Huda, "Mammographic feature enhancement by multiscale analysis," *IEEE Trans. Med. Imaging* **13**, 725–740 (1994).
34. A. Mencattini, M. Salmeri, R. Lojacono, M. Frigerio, and F. Caselli, "Mammographic images enhancement and denoising for breast cancer detection using dyadic wavelet processing," *IEEE Trans. Instrumentation and Measurement* **57**, 1422–1430 (2008).
35. P. Sakellaropoulos, L. Costaridou, and G. Panayiotakis, "A wavelet-based spatially adaptive method for mammographic contrast enhancement," *Phys. Med. Biol*. **48**, 787–803 (2003).

36. P. Heinlein, J. Drexl, and W. Schneider, "Integrated wavelets for enhancement of microcalcifications in digital mammography," *IEEE Trans. Med. Imaging* **22**, 402–413 (2003).
37. S. Skiadopoulos, A. Karahaliou, F. Sakellaropoulos, G. Panayiotakis, and L. Costaridou, "Breast component adaptive wavelet enhancement for soft-copy display of mammograms," *Proc. Digital Mammography*, 549–556, Manchester, UK (2006).
38. C.-M. Chang and A. Laine, "Coherence of multiscale features for enhancement of digital mammograms," *IEEE Trans. Information Technol. Biomed*. **3**, 32–46 (1999).
39. G. Derado, F. DuBois Bowman, R. Patel, M. Newell, and B. Vidakovic, "Wavelet image interpolation (WII): A wavelet-based approach to enhancement of digital mammography images," *Lecture Notes Comp. Sci.* **4463**, 203–214 (2007).
40. F. Y. M. Lure, P. W. Jones, and R. S. Gaborski, "Multiresolution unsharp masking technique for mammogram image enhancement," *Proc. SPIE* **2710**, 830–839 (1996) [doi: 10.1117/12.237989].
41. J. Scharcanski and C. R. Jung, "Denoising and enhancing digital mammographic images for visual screening," *Comp. Med. Imaging and Graphics* **30**, 243–254 (2006).
42. J. Tang, X. Liu, and Q. Sun, "A Direct Image Contrast Enhancement Algorithm in the Wavelet Domain for Screening Mammograms," *IEEE J. Selected Topics Signal Process*. **3**, 74–80 (2009).
43. W. Qian, L. P. Clarke, M. Kallergi, and R. A. Clark, "Tree-structured nonlinear filters in digital mammography," *IEEE Trans. Med. Imaging* **13**, 25–36 (1994).
44. S. DelMarco and S. Agaian, "The design of wavelets for image enhancement and target detection," *Proc. SPIE* **7351**, 735103 (2009) [doi: 10.1117/12.816135].
45. S. C. Nercessian, K. A. Panetta, and S. S. Agaian, "Multiresolution decomposition schemes using the parameterized logarithmic image processing model with application to image fusion," *EURASIP J. Adv. Signal Process 2011*, 1–17 (2011).
46. S. S. Agaian, K. A. Panetta, and S. C. Nercessian, "Image Fusion Using A Parameterized Logarithmic Image Processing Framework," Chapter 8 in *Image Fusion,* Osamu Ukimura, Ed., Intech, New York (2011).
47. F. Sahba and A. Venetsanopoulos, "Contrast enhancement of mammography images using a fuzzy approach," *Proc. IEEE EMBS 2008*, 2201-2204 (2008).
48. I. Stephanakis, G. Anastassopoulos, A. Karayiannakis, and C. Simopoulos, "Enhancement of medical images using a fuzzy model for segment dependent local equalization," *Proc. ISPA 2003*, 970–975 (2003).

49. J. Jiang, B. Yao, and A. M. Wason, "Integration of fuzzy logic and structure tensor towards mammogram contrast enhancement," *Comp. Med. Imaging and Graphics* **29**(1), 83–90 (2005).
50. Y. Zhou, K. Panetta, and S. Agaian, "Human visual system based mammogram enhancement and analysis," *Proc. IEEE Int. Conf. Image Process. Theory Tools Applications*, Paris, France, 229–234 (2010).
51. K. A. Panetta, E. J. Wharton, and S. S. Agaian, "Human Visual System-Based Image Enhancement and Logarithmic Contrast Measure," *IEEE Trans. Systems, Man and Cybernetics, Part B* **38**, 174–188 (2008).
52. E. Wharton, K. Panetta, and S. Agaian, "Adaptive multi-histogram equalization using human vision thresholding," *Proc. SPIE* **6497**, 64970G (2007) [doi: 10.1117/12.704474].
53. Y. Zhou, K. Panetta, and S. Agaian, "Human visual system based contrast enhancement for x-ray CT images using alpha weighted quadratic filter," *Proc. IS&T / SPIE Electronic Imaging 2010: Image Processing: Algorithms and Systems VIII*, San Jose, CA (2010).
54. S. Bakhtiari, S. Agaian, and M. Jamshidi, "An enhanced Empirical Mode Decomposition based method for image enhancement," *Proc. IEEE SMC 2011*, 2681–2686 (2011).
55. S. Bakhtiari, S. Agaian, and M. Jamshidi, "A novel empirical mode decomposition based system for medical image enhancement," *Proc. IEEE SysCon 2011*, 145–148 (2011).
56. S. Bakhtiari, S. Agaian, and M. Jamshidi, "Complex ensemble empirical mode decomposition and alpha-rooting for image contrast enhancement," *Proc. SPIE* **8063**, 806313 (2011) [doi: 10.1117/12.887424].
57. S. Bakhtiari, S. Agaian, and M. Jamshidi, "A color image enhancement method based on Ensemble Empirical Mode Decomposition and Genetic Algorithm," *World Automation Congress 2012*, 1–6 (2012).
58. S. M. Pizer, E. P. Amburn, J. D. Austin, R. Cromartie, A. Geselowitz, T. Greer, B. ter Haar Romeny, J. B. Zimmerman, and K. Zuiderveld, "Adaptive histogram equalization and its variations," *Comp. Vision, Graphics, Image Process*. **39**, 355–368 (1987).
59. R. C. Gonzalez and R. E. Woods, *Digital Image Processing*, 3rd ed., Prentice Hall, New York (2007).
60. E. Wharton, K. Panetta, and S. Agaian, "Human Visual System Based Multi-Histogram Equalization for Non-Uniform Illumination and Shoadow Correction," *Proc. IEEE ICASSP 2007*, I-729–I-732 (2007).
61. L. Lu, Y. Zhou, K. Panetta, and S. Agaian, "Comparative study of histogram equalization algorithms for image enhancement," *Proc. SPIE* **7708**, 770811 (2010) [doi: 10.1117/12.853502].

62. Y. Zhou, K. Panetta, and S. Agaian, "3D CT baggage image enhancement based on order statistic decomposition," *Proc. IEEE Technol. Homeland Security 2010*, Waltham, MA (2010).
63. K. Panetta, S. Agaian, Y. Zhou, and E. J. Wharton, "Parameterized Logarithmic Framework for Image Enhancement," *IEEE Trans. Systems, Man and Cybernetics, Part B* **41**, 460–473 (2011).
64. K. Panetta, E. Wharton, and S. Agaian, "Logarithmic Edge Detection with Applications," *J. Comp*. **3**, 11–19 (2008).
65. M. Jourlin and J. Pinoli, "A model for logarithmic image processing," *J. Microscopy* **149**, 21–35 (1988).
66. M. Jourlin and J.-C. Pinoli, "Image dynamic range enhancement and stabilization in the context of the logarithmic image processing model," *Signal Process*. **41**, 225–237 (1995).
67. N. Petrick, H.-P. Chan, B. Sahiner, and D. Wei, "An adaptive density-weighted contrast enhancement filter for mammographic breast mass detection," *IEEE Trans. Med. Imaging* **15**, 59–67 (1996).
68. E. J. Wharton, K. A. Panetta, and S. S. Agaian, "Edge Preserving Image Enhancement Using Anisotpic Diffusion," *Proc. SPIE* **6812**, 681218 (2008) [doi: 10.1117/12.766893].
69. C. Gao, K. Panetta, and S. Agaian, "A new color contrast enhancement algorithm for robotic applications," *Proc. IEEE Technol. Practical Robot Applications 2012*, 42–47 (2012).
70. R. G. Kogan, S. S. Agaian, and K. Panetta, "Visualization using rational morphology and zonal magnitude reduction," *Proc. SPIE* **3304**, 153–163 (1998) [doi: 10.1117/12.304595].
71. A. P. Dhawan, G. Buelloni, and R. Gordon, "Enhancement of Mammographic Features by Optimal Adaptive Neighborhood Image Processing," *IEEE Trans. Med. Imaging* **5**, 8–15 (1986).
72. V. H. Guis, M. Adel, M. Rasigni, G. Rasigni, B. Seradour, and P. Heid, "Adaptive neighborhood contrast enhancement in mammographic phantom images," *Opt. Eng*. **42**(2), 357–366 (2003) [doi: 10.1117/1.1534846].
73. G. Ramponi, N. K. Strobel, S. K. Mitra, and T.-H. Yu, "Nonlinear unsharp masking methods for image contrast enhancement," *J. Electron. Imaging* **5**(3), 353–366 (1996) [doi: 10.1117/12.242618].
74. Z. Wu, J. Yuan, B. Lv, and X. Zheng, "Digital mammography image enhancement using improved unsharp masking approach," *Proc. IEEE CISP 2010*, 668–672 (2010).
75. G. Ramponi and A. Polesel, "Rational unsharp masking technique," *J. Electron. Imaging* **7**(2), 333–338 (1998) [doi: 10.1117/1.482649].
76. J. George and S. P. Indu, "Fast Adaptive Anisotropic Filtering for Medical Image Enhancement," *Proc. IEEE ISSPIT 2008*, 227–232 (2008).

77. A. Polesel, G. Ramponi, and V. J. Mathews, "Image enhancement via adaptive unsharp masking," *IEEE Trans. Image Process*. **9**, 505–510 (2000).
78. N. Strobel and S. K. Mitra, "Quadratic filters for image contrast enhancement," *Proc*. *Signals, Systems and Computers 1994*, 208–212 (1994).
79. G. Ramponi, "A cubic unsharp masking technique for contrast enhancement," *Signal Process*. **67**, 211–222 (1998).
80. S. Singh and K. Bovis, "An evaluation of contrast enhancement techniques for mammographic breast masses," *IEEE Trans. Information Technol. Biomed*. **9**, 109–119 (2005).
81. S. Agaian, K. Panetta, and A. Grigoryan, "A new measure of image enhancement," *Proc*. *Int. Conf. Signal Process. Comm.*, 19–22, Marbella, Spain (2000).
82. S. S. Agaian, "Visual morphology," *Proc. SPIE* **3646**, 139–150 (1999) [doi: 10.1117/12.341081].
83. E. Wharton, S. Agaian, and K. Panetta, "Comparative study of logarithmic enhancement algorithms with performance measure," *Proc. SPIE* **6064**, 606412 (2006) [doi: 10.1117/12.647489].
84. E. Wharton, K. Panetta, and S. Agaian, "Human visual system based similarity metrics," *Proc. IEEE Systems, Man and Cybernetics 2008*, 685–690 (2008).
85. J. Tang, E. Peli, and S. Acton, "Image enhancement using a contrast measure in the compressed domain," *IEEE Signal Process. Lett*. **10**, 289–292 (2003).
86. ITU-T, "Methods for subjective determination of transmission quality," *Recommendation*, International Telecommunication Union, p. 800 (1996).
87. J. Suckling, J. Parker, D. Dance, S. Astley, I. Hutt, C. Boggis, I. Ricketts, E. Stamatakis, N. Cerneaz, and S. Kok, "The mammographic image analysis society digital mammogram database," *Proc. 2nd Int. Workshop Digital Mammography*, 375–378 (1994).
88. M. K. Kundu and S. K. Pal, "Thresholding for edge detection using human psychovisual phenomena," *Pattern Recognition Lett*. **4**, 433–441 (1986).
89. G. Buchsbaum, "An analytical derivation of visual nonlinearity," *IEEE Trans. Biomed. Eng*. **27**, 237–242 (1980).
90. M. J. P. Castanho, L. C. Barros, A. Yamakami, and L. L. Vendite, "Fuzzy receiver operating characteristic curve: an option to evaluate diagnostic tests," *IEEE Trans. Information Technol. Biomed*. **11**, 244–250 (2007).
91. M. Zweig and G. Campbell, "Receiver-operating characteristic (ROC) plots: a fundamental evaluation tool in clinical medicine," *Clin. Chem*. **39**, 561–577 (1993).

92. Wikipedia, "Receiver operating characteristic," http://en.wikipedia.org/wiki/Receiver_operating_characteristic.
93. A. Slaby, "ROC analysis with MATLAB," *Proc. 29th Int. Conf. Information Technol. Interfaces*, Cavtat, Croatia, 191–196 (2007).
94. J. Eng, "ROC analysis: web-based calculator for ROC curves," available at http://www.jrocfit.org (2007).

Yicong Zhou received his B.S. degree from Hunan University, Changsha, China, and his M.S. and Ph.D. degrees from Tufts University, Medford, MA, USA, all in Electrical Engineering. He is currently an Assistant Professor in the Department of Computer and Information Science at the University of Macau, China. Dr. Zhou is a member of the IEEE and SPIE. His research interests include multimedia security, image and signal processing, pattern recognition, and medical imaging.

Sos Agaian is the Peter T. Flawn Professor of Electrical and Computer Engineering at the University of Texas, San Antonio, and a professor at the University of Texas Health Science Center, San Antonio. Dr. Agaian received his M.S. degree (summa cum laude) in Mathematics and Mechanics from Yerevan State University, Armenia; his Ph.D. in Mathematics and Physics from the Steklov Institute of Mathematics, Russian Academy of Sciences (RAS); and his Eng.Sc.D. from the Institute of Control Sciences, RAS. He has authored more than 500 scientific papers, seven books, and holds 14 patents. He is a Fellow of SPIE, the American Association for the Advancement of Science (AAAS), and Imaging Sciences and Technology (IS&T). He also serves as a foreign member of the Armenian National Academy. He is the recipient of MAEStro Educator of the Year, sponsored by the Society of Mexican American Engineers. The technologies that Dr. Agaian invented have been adopted by multiple institutions, including the U.S. government, and commercialized by industry. He is an Editorial Board Member for the *Journal of Pattern Recognition and Image Analysis* and an Associate Editor for several journals, including the *Journal of Electronic Imaging* (SPIE, IS&T) and *System* (Elsevier). His research interests include multimedia processing, imaging systems, information security, artificial intelligence, computer vision, 3D imaging sensors, fusion, and biomedical and health informatics.

Karen Panetta received her B.S. degree in Computer Engineering from Boston University, Boston, MA, and her M.S. and Ph.D. in Electrical Engineering from Northeastern University, Boston. Dr. Panetta is currently a Professor in the Department of Electrical and Computer Engineering at Tufts University, Medford, MA, and director of the Simulation Research Laboratory. She is the Editor-in-Chief of the IEEE *Women in Engineering Magazine*. Dr. Panetta is the IEEE-USA Vice President of Communications and Public Affairs; she also served as the 2011 chair of the IEEE Boston Section, which has over 8800 members. During 2007–2009, she served as the worldwide director for IEEE Women in Engineering, overseeing the world's largest professional organization supporting women in engineering and science. She is a Fellow of the IEEE, and she is also the recipient of the 2012 IEEE Ethical Practices Award and the Harriet B. Rigas Award for Outstanding Educator. In 2011, Dr. Panetta was awarded the Presidential Award for Engineering and Science Education and Mentoring by U.S. President Obama. Her research focuses on developing efficient algorithms for simulation, modeling, signal, and image processing for biomedical and security applications.

C. L. Philip Chen received his M.S. degree from the University of Michigan, Ann Arbor, Michigan, USA and his Ph.D. from Purdue University, West Lafayette, Indiana, USA, both in Electrical Engineering. Dr. Chen is currently a Chair Professor and the Dean of Faculty of Science and Technology at the University of Macau, China. He was a Professor and Chair of the Department of Electrical and Computer Engineering, as well as the Associate Dean for Research and Graduate Studies of the College of Engineering at the University of Texas in San Antonio after he served as an assistant, an associate, and a full professor in the Department of Computer Science and Engineering at Wright State University, Dayton, OH. Dr. Chen has served as a member of organizing committees for many IEEE conferences under different capacities. He is currently the President of the IEEE SMC Society. He is an Accreditation Board of Engineering and Technology Education (ABET) Program Evaluator for computer engineering, electrical engineering, and software engineering programs. He is a fellow of the IEEE and AAAS. His research interests include computer networking, neural networks, fuzzy neural systems, intelligent systems, robotics, and CAD/CAM.